Experimental and Numerical Study of Unsteady Wakes Behind an Oscillating Car Model

Emmanuel GUILMINEAU[1] **and Francis CHOMETON**[2]

[1] *Laboratoire de Mécanique des Fluides, CNRS UMR 6598, Ecole Centrale de Nantes*
BP 92101, 44321 Nantes Cedex 3, France
[2] *Laboratoire d'Aérodynamique, Conservatoire National des Arts et Métiers*
15 rue Marat, 78210 Saint Cyr l'Ecole, France

Abstract. This research focuses on the analysis of the instability of passenger vehicles associated with transient crosswind gusts. A new vehicle model, created to analyze the behavior of unsteady wakes on bluff bodies, is proposed. This test model called Willy is designed using the following criteria: the geometry is realistic compared to a real vehicle, the model's plane under-body surface is parallel to the ground, and the separations are limited to the region of the base for a moderated yaw angle. In the present paper, the tests are performed on the model animated by an oscillating yaw angle at a frequency of 2 Hz in a steady wind. Experiments are carried out at Reynolds number of 0.9×10^6 at the Conservatoire National des Arts et Métiers and computations are performed at the Ecole Centrale de Nantes. The numerical results are compared with experimental data.

Key words: automotive flow, crosswind, transient gust, incompressible flow.

1. Introduction

The aerodynamic characteristics of a vehicle and their evolution as a function of situations such as passing, crossing, the presence of an unsteady gust of wind or of a non uniform turbulent atmospheric flow are factors in the vehicle's on-road stability and of the safe manoeuvrability appreciated by the driver [7]. The simplest way to define the stability of a vehicle is to measure the steady forces and moments in a wind tunnel as a function of the yaw angle β. The knowledge of the lift or weight forces at the level of the wheels axes and of the forces and moments on the body allows to define the position of the lateral thrust center in comparison with the center of gravity. This result can be improved by introducing these steady aerodynamic data in a dynamic model that includes the dynamic of the suspension, springing and tyres. This approach postulates that there is no phenomena of phase shifting or hysteresis and actually a dynamic approach is necessary in order to prove that these phenomena do not exist or remain weak compared to others. Experimental studies in a wind tunnel or on the road of the dynamic behaviour of vehicles are in counterpart very complex and much analysis must be performed on models. Several techniques allow the reproduction of a side gust of wind in a wind tunnel, assimilated to a pulse of velocity. For Macklin *et al.* [12], it was obtained by propelling the model on a rail crossing the test section of the wind tunnel. Ryan *et al.* [15], used a technique where the side wind was produced by a cross jet. Another technique, more easily set up, consists of submitting the model to a periodic movement in a steady

wind. This approach does not actually simulates the situation of passing but it does bring into evidence the phenomena of phase shifting or hysteresis and allows their analysis [4]. This last approach was retained here [1]. More complicated problems like vehicle passing or crossing were correctly analysed on 1/5 scale models propelled on a rail [14]. The transient aerodynamic effects experienced by every member of a platoon during passing manoeuvres were also analysed by Tsuei *et al.* [17] on 1/20 scale models. The same techniques are also applied to the analysis of cross winds effects on high-speed trains [16].
To date, accuracy of numerical simulation has been improved and simulation is now widely used in the automotive industry for exploration of flow physics or for effort prediction on full scale vehicles. Many of the CFD tests are done at at zero yaw angle for steady flows and use simplified bluff bodies [10] or the reference Ahmed car model [9, 11]. More recently a new model (the Willy car model) was proposed and experimented for steady and unsteady conditions. The unsteady results showed phenomena of phase shift and hysteresis [3]. A detailed comparison between numerics and experiments were done on this model at large yaw angles up to $\beta = 30°$ for steady flows [5, 6]. Comparisons show a good agreement between numerics and experiments.
Experimental and numerical data presented in this paper are concerned with the analysis of unsteady flows around the Willy model. The tests are performed on the model animated by an oscillating yaw angle of amplitude $\Delta\beta = 10°$ in a steady wind at a Reynolds number of 0.9×10^6. The experimental unsteady wall pressures are compared to the numerical results for a frequency f = 2 Hz. The post-processing of other numerical data allows the understanding of the physics of phase shifting phenomena observed on wall pressures.

2. Test Model

Experimental and numerical tests are performed on the squareback Willy test model, which is realistic, compared to a van-type vehicle. A complete definition of the model is given in reference [2]. The main characteristics are as follows, see Figure 1:

- The geometry is realistic, compared to a real van-type vehicle,
- The model's plane underbody surface is parallel to the ground,
- The separations are limited to the region of the base for a moderated yaw angle, i.e. $\beta = 10°$,
- The digital definition of the model allows the modification of the shape through only 4 parameters given in [2].

The overall length of the model is L1 = 675 mm, the width 240 mm, the maximum height 192 mm and its surface reference is the maximum cross section $S_{ref} = 41791$ mm^2. The ground clearance is G = 29 mm and the diameter of the four feet (f) which are used to secure the model to the floor of the wind tunnel is $\phi 1 = 20$ mm. All dimensions are defined in the Table 1. In previous steady analysis [6], a cylinder of diameter 40 mm located under the body was used to protect the pressure tubes passing from the pressure taps to the multi-manometer. This tube modifies strongly the flow around the model and was removed for the present unsteady experimental and numerical tests. The reference axis of the model is the Eiffel axis where the axis

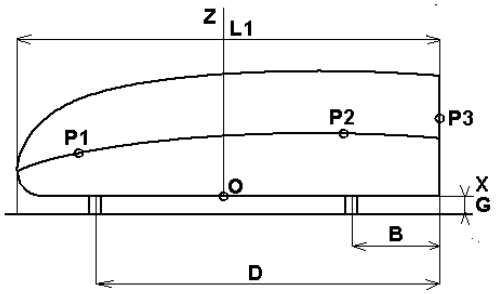

(a) Side view

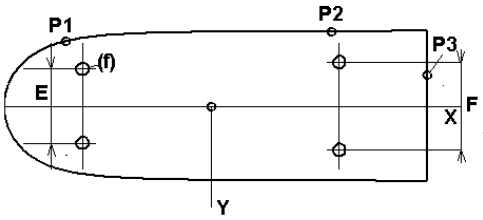

(b) Bottom view

Figure 1. Model definition

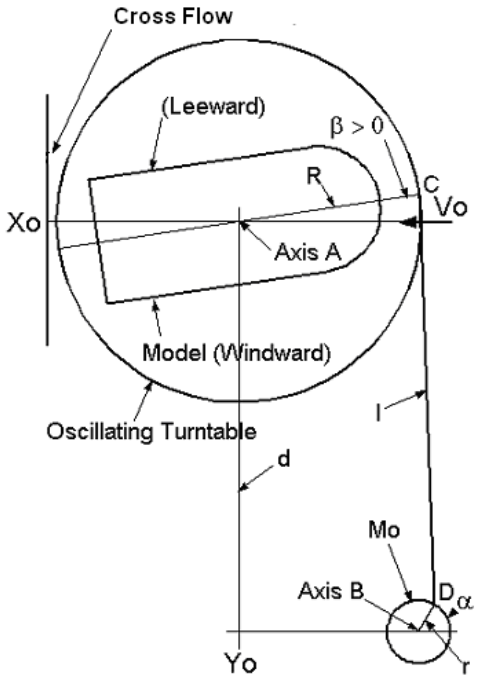

Figure 2. Oscillating bench

Table 1. Dimensions of the test model (data in mm and mm^2)

L1	B	D	E	F	G	H	$\phi 1$	S_{ref}
675	140	550	118	140	29	345	20	41791

is parallel to the upstream velocity V_0. The origin of axis lies at the point O located on the floor of the model, see Figure 1. This point O is the centre of rotation of the model when submitted to a harmonic oscillation.

3. Experimental Set-Up

Wall pressures measurements are performed in a Prandtl-type wind tunnel of the CNAM. The semi-open test section has a cross section of 1.45 m by 1.45 m and the ground of the wind tunnel is fixed. The wind tunnel is equipped with a six components balance. The value of the yaw angle β is positive when the right side of the car model is windward. The turbulence level at the centre of the test section is 2%. For an upstream velocity $V_0 = 20$ m/s, the thickness of the turbulent boundary layer at a point located on the floor of the wind tunnel, at x = -670 mm, i.e. upstream the body, and y = 10 mm is $\delta = 40$ mm with a shape factor H = 1.29. This data is obtained with the model at a yaw angle of $\beta = 30°$. The experimental results given in the paper are obtained at a Reynolds number of 0.9×10^6 based on the velocity V_0 and the length L1 of the model.
The set-up allowing the model to be put into movement at the frequency f is described in Figure 2. The model is attached to a turntable (T) oscillating around its

z axis (A). A rod (CD) of length l is attached to the disc of a step motor (Mo). The set-up is conceived so that the rod was parallel to axis y when $\beta = \Delta\beta$; in these conditions, $r = R \sin \Delta\beta$ and $l = d$. With r = 0.0255 m and $l = d = 0.3264$ m, the movement $\beta = f(\alpha)$ is close to the sine function. For an angle $\alpha = \omega t$, where ω is a constant angular velocity and t the time, the actual movement $\beta = f(\alpha)$ is the physical root of:

$$a \tan^2\left(\frac{\beta}{2}\right) + b \tan\left(\frac{\beta}{2}\right) + c = 0 \tag{1}$$

where:

$$a = A + B\left(\cos\Delta\beta + \frac{\cos\alpha}{\sin\Delta\beta}\right) \quad b = B\left(\frac{2l\sin\Delta\beta}{r} - 2\sin\Delta\beta\sin\alpha\right) \tag{2}$$

$$c = A - B\left(\cos\Delta\beta + \sin\Delta\beta\cos\alpha\right) \tag{3}$$

$$A = B\left(1 + 0.5\sin 2\Delta\beta\cos\alpha\right) - 2rl\sin\alpha \qquad B = \frac{2r^2}{\sin^2\Delta\beta} \tag{4}$$

Wall pressures are measured along the curve (A) of the model, see Figure 1. The internal diameter of the pressure taps is 1.5 mm. Pressure coefficients Cp are defined by:

$$Cp = \frac{p - p_0}{\frac{1}{2}\rho V_0^2} \tag{5}$$

where p_0 and p are respectively the upstream static pressure and the local pressure. Steady and unsteady pressure measurements are performed with dynamic differential pressure sensors Honeywell DC010BDC4 with pressure range ± 10 mb. Sensors are mounted inside the model and the electric wires pass through a foot (f). The frequency response of this device was tested in a shock tube which was modified in order to provide weak shock waves suitable with the pressure range of the sensors. The natural frequency of the actual measurement device is 520 Hz. The bandwidth frequency at which the error is 5% is about 30 Hz.
Concerning the post processing of unsteady pressures, the phase shifting introduced by the mechanisms and the angle triggering is calculated on quasi-steady reference results obtained at a low frequency $f = 0.1$ Hz. It was admitted that this angle adjustment is independent of the frequency and applied to all tests.

4. Numerics

4.1. Flow Solver

The ISIS-CFD flow solver, developed by the EMN (Equipe Modélisation Numérique) of the Fluid Mechanics Laboratory of the Ecole Centrale of Nantes, uses the incompressible unsteady Reynolds-averaged Navier-Stokes equations (RANSE). The solver is based on the finite volume method to build a spatial discretization of the transport equations.
The face-based method is generalized to two-dimensional or three-dimensional unstructured meshes for which non-overlapping control volumes are bounded by an arbitrary number of constitutive faces. The velocity field is obtained from the momentum conservation equations and the pressure field is extracted from the mass conservation constraint, or continuity equation, transformed into a pressure-equation. A

second-order accurate three-level fully implicit time discretization is used and surface and volume integrals are evaluated using second-order accurate approximation [8]. In the case of turbulent flows, additional transport equations for modeled variables are solved in a form similar to that of the momentum equations and they can be discretized and solved using the same principles. In this study, the turbulence model used is the $K-\omega$ SST model of Menter [13].
To take account of the oscillation of the model, all mesh points move with the same velocity than the one of the car model. However, this approach does not represent the experimental set-up because in experiments, the model is attached to a turntable and in this case, it is not all the ground that oscillates. We suppose that this different approach in numerics does not induce some secondary effects.

4.2. Mesh

The computational domain starts 3.5×L1 in front of the model and extends 4×L1 behind the model. The width of the domain extends from +1000 mm (1.48×L1) to -1000 mm and the height is 1050 mm (1.55×L1). The mesh is generated by using HEXPRESS^{TM}, an automatic unstructured mesh generator. This software generates meshes only containing hexaedrals. The mesh is composed to about 6.3 millions of points with approximatively 93000 points on the model and 48100 points on the wind tunnel floor. For the model, we use the near-wall low-Reynolds number turbulence model, the distance between the body and the first fluid points is fixed to 0.006 mm, i.e. $y^+ = 0.5$. For the wind tunnel floor, we use a wall function, and the distance between the floor and the first fluid points is fixed to 0.6 mm.

5. Results

Experimental and numerical results given in this paper are obtained for $\Delta\beta = 10°$ and a oscillation frequency $f = 2$ Hz i.e. a Strouhal number $St = 0.07$ calculated with the upstream velocity V_0 and the lenght L1 of the model. For the simulation, the time step used is $\Delta t = 0.001$ s.

5.1. Unsteady forces and moments

The numerical and experimental forces Cx0 and Cy0 drawn in Figures 3 and 4 are respectively the drag and the side forces coefficients in the Eiffel axes linked to upstream velocity Vo . The labels [1] to [10] drawn in the unsteady curves indicate the evolution of the angle β along a complete cycle. The experimental static values of Cx0 = f(β) and Cy0 = f(β) are also given as well as the numerical static values calculated at $\beta = 0°$ and $\beta = 10°$. These results show that, for a low value of the Strouhal number St = 0.07, the unsteadiness of the flow introduces a phase shift effect for Cx0 and Cy0 and increases the value of the drag, particularly around $\beta = 0°$. In counterpart the value of d(Cy0)/dβ does not change. In the same way, the sign of d(CN)/dβ, where CN is the yaw coefficient, does not change, and the unsteadiness does not modify the stability of the model. The interest of the polar curve Cy0 = f(Cx0) drawn in Figure 6 is to show that the dynamic thickness ε = Cy0/Cx0 of the model, presented in Figure 7, is maximum, about $\varepsilon = 1.27$

for $\beta = -6.95°$ located between the labels [9] and [10]. At the same yaw angle $\beta = -6.95°$ the static value of the thickness is about $\varepsilon = 0.78$.

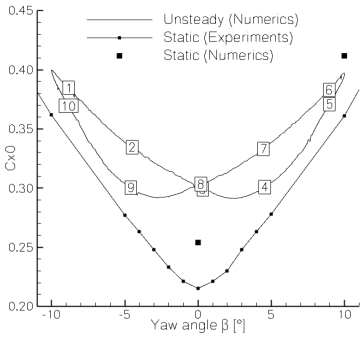

Figure 3. $Cx0 = f(\beta)$

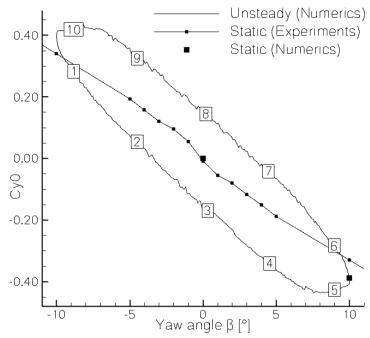

Figure 4. $Cy0 = f(\beta)$

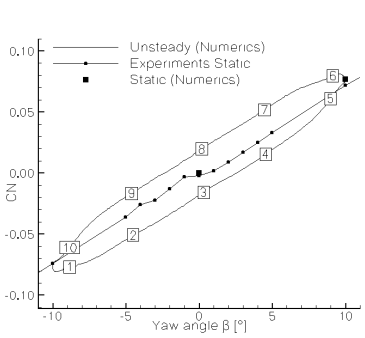

Figure 5. $CN = f(\beta)$

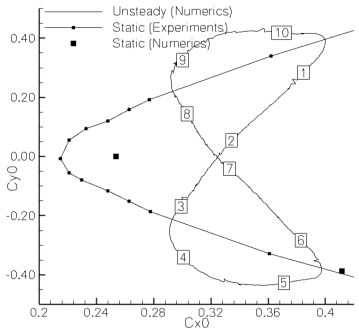

Figure 6. $Cy0 = f(Cx0)$

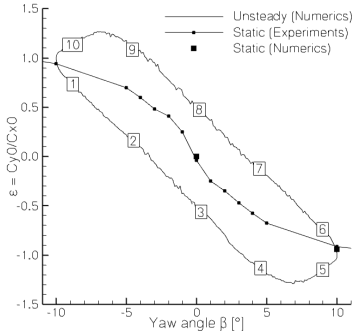

Figure 7. $\varepsilon = f(\beta)$

5.2. Wall pressures

The comparison between the experimental and calculated wall pressure are given in Figures 8 for two pressure taps noted P1, P2 located on the curve (A) of the model, and a third tap P3 located on its base, see Figure 1. The agreement is very good and confirms the results obtained for the forces and moments. The three results show clearly a phase shift phenomena with no non-linear effects. At location P1 which is at the level of the nose of the model, the phase shift is very low, close to zero but increases along the line (A). At location P2 the shape of the curve obtained for the unsteady pressure is identical to the curve for the unsteady side force Cy0. In the same way the loop observed for the drag Cx0 is also observed for the base pressure.

5.3. Unsteadiness effects in the wake

For cross flows, the rotation of vortices is defined for an observer looking the model backward. For each frame the number into the brackets corresponds to the label drawn in Figures 3 to 7. The sense of the loop is also given. The unsteadiness and temporal variation of the wake along a cycle from $\beta = -10°$ to $\beta = +10°$ and then from $\beta = +10°$ to $\beta = -10°$ is described in Figures 9 for several yaw angles. The

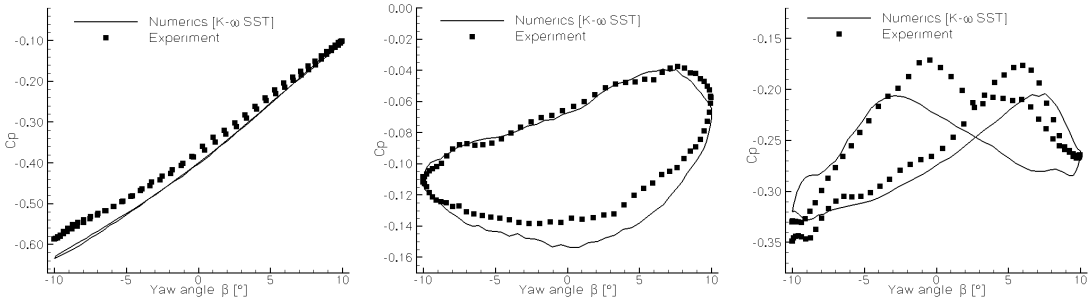

(a) Pressure tap P1 (b) Pressure tap P2 (c) Pressure tap P3

Figure 8. Pressure coefficient CP = f(β)

flow is analysed through cross flow velocities drawn at X/L1 = 0.70. The reading of these results must take into account that the vortices which appear at X/L1 = 0.70 are shed at the level of the base located at X/L1 = 0.5. This figure shows that the pair of vortices observed on frames [1], [2] and [3] vanish in frame [4] and are replaced in frame [5] by a new pair of symmetrical vortices. The phenomena is the same for the frames evoluting from [6] to [10].
At $\beta = +4.56°$ and $+4.59°$ which are roughly at half-cycle, the results described in Figure 9 show that no vortex are visible in the cross section. The detail of the modification of the wake is described in Figure 10. In this figure the first line of frames must be read from left to right, the second line from right to left, and the last from left to right. At $\beta = +2.18°$, the vortex V1 is visible but the vortex V2 is weak; at $\beta = +2.79°$ only the clockwise vortex V1 is present. At $\beta = +3.39°$ no vortex appear in the cross flow. At $\beta = +5.11°$, a counterclock vortex V3 appears and grows up as seen in the following frames. At angle $\beta = +6.65°$ a new vortex V4 is rolling up, and form a vortex pair with the vortex V3 at $\beta = +7.12°$.
A comparison of the cross flow velocity vectors drawn at X/L1 = 0.70 at $\beta = 0°$ in static and in dynamic is given in Figure 11 for steady and unsteady flows. In static there are two symmetrical vortices V1 and V2, see the central frame . These two vortices are due to the facts that the base of the model is not circular and that the wake interacts with the fixed ground. In dynamic, the angular velocity of the model is maximum at $\beta = 0°$, and only the clockwise vortex V1 appears when it moves from $-10°$ to $+10°$, see the left frame. When the model is moving back from $\beta = +10°$ to $\beta = -10°$, only the counter-clockwise vortex V2 appears, see the right frame. The two wakes are symmetrical about the (x,z) plane and the drags Cxo are the same for the two dynamic situations, see Figure 3.

6. Conclusions

This paper presents the simulations and experiments of the flow around the Willy car model submitted to a harmonic oscillation at a Strouhal number $St = 0.07$ and an amplitude $\Delta\beta = 10°$. Unsteady experimental wall pressures, used as reference, has been carried out at the CNAM. For the numerics, the ECN ISIS-CFD is used with $K - \omega$ SST turbulence model. The results confirms that even at low frequency and low amplitude, there are phase shift effect phenomena associated with an increase of the drag, particularly at $\beta = 0°$ where the angular velocity of the model is maximum. Comparisons show a good agreement between numerics and experiments,

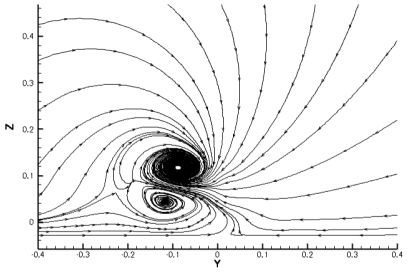

[1]: $\beta = -8.83°$, from $-10°$ to $+10°$

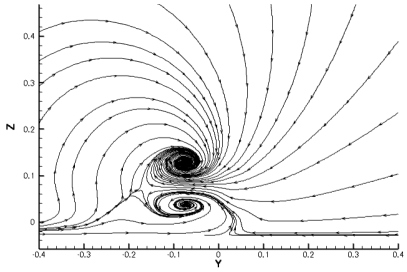

[10]: $\beta = -8.85°$, from $+10°$ to $-10°$

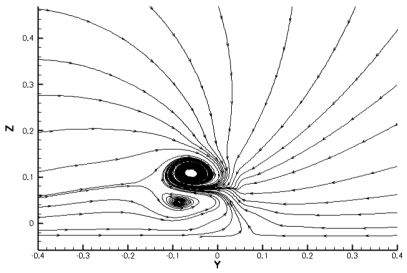

[2]: $\beta = -4.50°$, from $-10°$ to $+10°$

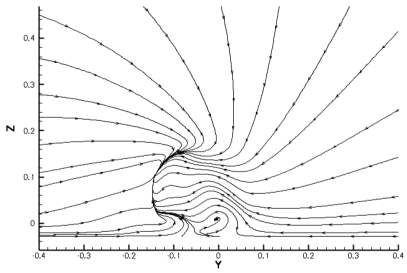

[9]: $\beta = -4.59°$, from $+10°$ to $-10°$

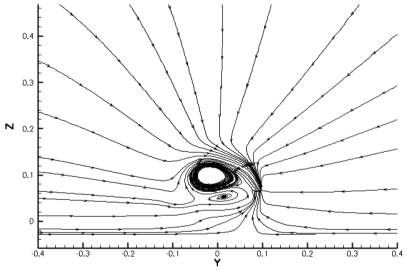

[3]: $\beta = +0.31°$, from $-10°$ to $+10°$

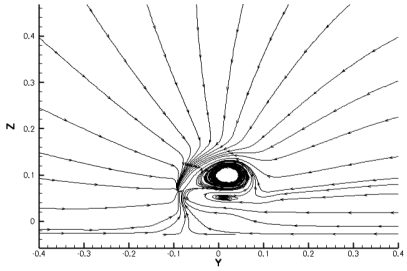

[8]: $\beta = +0.19°$, from $+10°$ to $-10°$

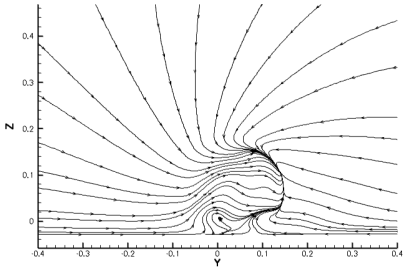

[4]: $\beta = +4.56°$, from $-10°$ to $+10°$

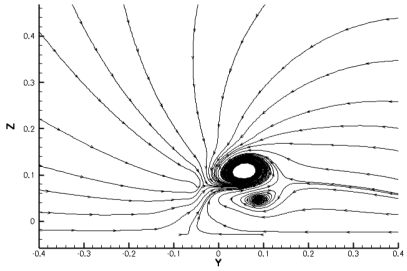

[7]: $\beta = +4.46°$, from $+10°$ to $-10°$

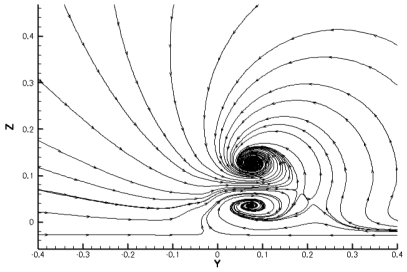

[5]: $\beta = +8.98°$, from $-10°$ to $+10°$

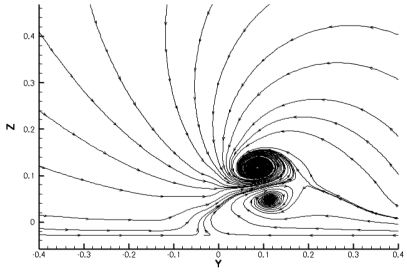

[6]: $\beta = +8.97°$, from $+10°$ to $-10°$

Figure 9. Unsteady cross flows at X/L1 = 0.70 for a full cycle

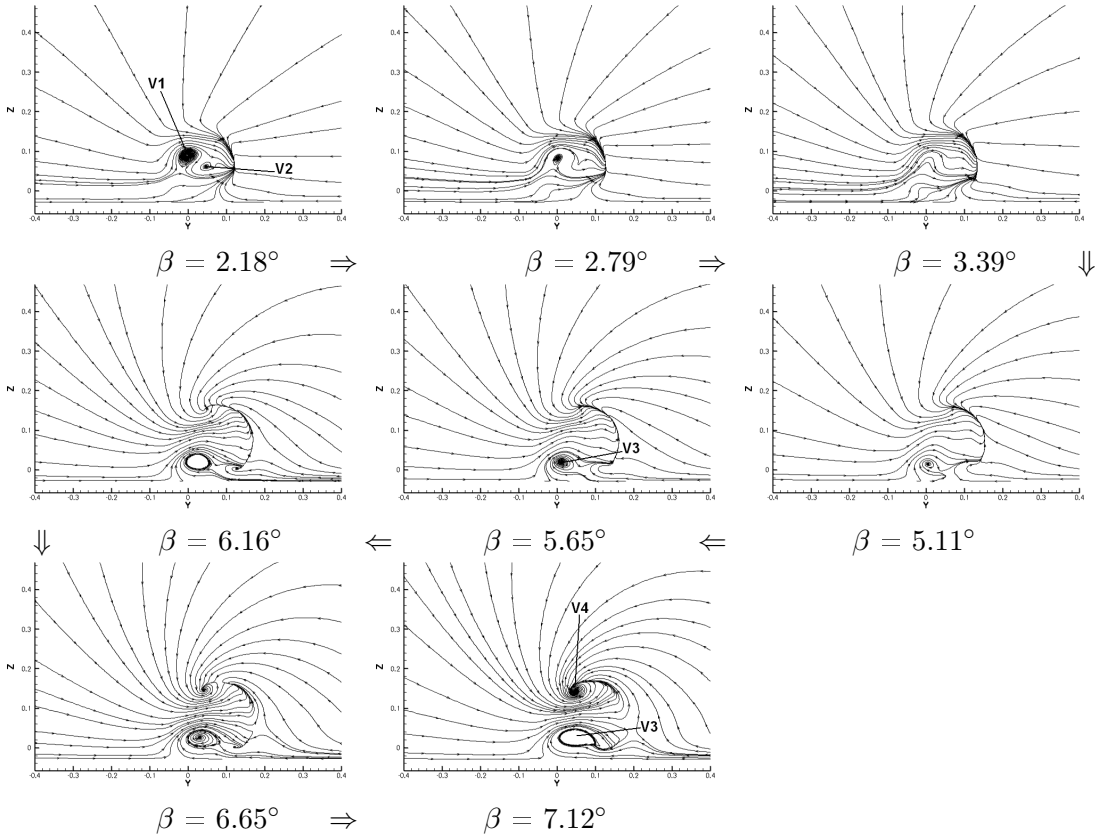

Figure 10. Cross flows at X/L1 = 0.70, detail of the wake

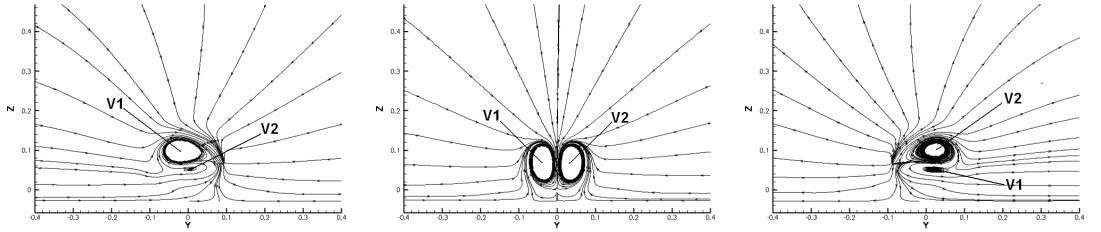

Figure 11. Steady and unsteady cross flows at $\beta = 0°$ and at X/L1 = 0.70

and confirm the capability of the ECN ISIS-CFD code to catch hysteresis or phase shift phenomena for 3D flows. Moreover, this approach shows that, after a validation of numerical results by experiments, the post-processing of numerical results gives access to a large lot of data allowing a fructuous analysis of flow physics. This project is performed in the framework of a collaboration between the Ecole Centrale de Nantes, the Conservatoire National des Arts et Métiers and the Ecole Nationale Supérieure de l'Aéronautique et de l'Espace (SUPAERO).

Acknowledgements

Experiments were performed by Mr. Jean-Luc Alleau in the framework of preparation for an engineering degree from the CNAM. We would like to thank Mr. E.

Aïssaoui for his help and cooperation. The authors gratefully acknowledge the Scientific Committee of IDRIS (project 0129) and of CINES (project dmn2049) for the attribution of CPU time.

References

[1] F. Chometon and P. Gilliéron. Analysis of unsteady wakes by images processing in automotive aerodynamics. In *Congress FLUCOME*, Tokyo, Japan, 1997.

[2] F. Chometon, A. Strzelecki, V. Ferrand, H. Dechipre, P.C. Dufour, M. Gohlke, and V. Herbert. Experimental study of unsteady wakes behind an osci. SAE Technical Paper 2005-01-0604, 2005.

[3] F. Chometon, A. Strzelecki, J. Laurent, and E. Aïssaoui. Experimental analysis of unsteady wakes on a new simple car model. In *Fifth International Colloquium on Bluff Body Aerodynamics and Applications*, pages 545–548, Ottawa, Ontario, Canada, 2004.

[4] K.P.K. Garry and K.R. Cooper. Comparison of quasi-static and dynamic wind tunnel measurements on simplified tractir-trailer models. *Journal of Wind Engineering and Industrial Aerodynamics*, 22:185–194, 1986.

[5] E. Guilmineau. Numerical simulation of wakes behind a car model. In *FISITA World Automotive Congress*, Yokohama, Japan, 2006.

[6] E. Guilmineau and F. Chometon. Experimental and numerical analysis of the effect of side wind on a simplified car model. SAE Techincal Paper 2007-01-0108, 2007.

[7] W.H. Hucho. *Aerodynamics of road vehicles.* SAE International, 1998.

[8] H. Jasak, H.G. Weller, and A.D. Gosman. High resolution nvd differencing scheme for arbitrarily unstructured meshes. *International Journal for Numerical Methods in Fluids*, 31:431–449, 1999.

[9] S. Kapadia, S. Roy, and K. Wurtzler. Detached eddy simulation over a reference Ahmed car model. In *41st Aerospace Sciences Meeting and Exhibit*, AIAA Paper 2003-0857, Reno, NE, January 2003.

[10] B. Khalighi, S. Zang, C. Koromilas, S.R. Balkany, L.P. Bernal, G. Laccarino, and P. Moin. Experimental and computational study of unsteady wake flow behind a bluff body with drag reduction device. SAE Technical Paper 2001-01B-207, 2001.

[11] S. Krajnovic and L. Davidson. Flow around a simplified car - part 1: Large eddy simulation. *Journal of Fluids Engineering*, 127:907–918, 2005.

[12] A.R. Macklin, K.P. Garry, and J.P. Howell. Comparing static and dynamic testing techniques for the crosswind sensitivity of road vehicles. SAE Technical Paper 960674, 1996.

[13] F.R. Menter. Zonal two-equation $k-\omega$ turbulence models for aerodynamic flows. In *AIAA 24th Fluid Dynamics Conference*, AIAA Paper 93-2906, Orlando, FL, July 1993.

[14] C. Noger, C. Regardin, and E. Szechenyi. Investigation of the transient aerodynamic phenomena associated with passing manoeuvres. *Journal of Fluids and Structures*, 21:231–241, 2005.

[15] A. Ryan and R.G. Dominy. The aerodynamic forces induced on a passenger vehicle in response to a transient cross-wind gust at a relative incidence of 30°. SAE Technical Paper 980392, 1998.

[16] S. Sanquer, C. Barré, M. Dufresne de Virel, and L.M. Cléon. Effect of cross winds on high-speed trains: development of a new experimental methodology. *Journal of Wind Engineering and Industrial Aerodynamics*, 92:535–545, 2004.

[17] L. Tsuei and Ö. Savas. A wind tunnel investigation of the transient aerodynamic effects on a four-car platoon during passing manoeuvers. SAE Paper 2000-01-0875, 2000.